12th INTERNATIONAL SCIENTIFIC CONFERENCE ON DEFENSIVE TECHNOLOGIES
OTEH 2026
Serbia, Tara, 21 - 24 October 2026

HIGH-PRESSURE JET SUPPLY SYSTEM FOR POWERED WIND TUNNEL MODELS: CALIBRATION AND PERFORMANCE

BILJANA ILIĆ
Military Technical Institute, Belgrade, biljana.ilic@icloud.com

MARIJA SAMARDŽIĆ
Military Technical Institute, Belgrade, marija.samardzic.vti@gmail.com

BOŽIDAR SIMOVIĆ
Military Technical Institute, Belgrade, simovic.bozidar@gmail.com

ISIDORA STANKOVIĆ
Military Technical Institute, Belgrade, stank151.dora@gmail.com

OGNJEN BABIĆ
Military Technical Institute, Belgrade, ognjen813@gmail.com

GORAN OCOKOLJIĆ
Military Technical Institute, Belgrade, ocokoljic.goran@gmail.com

Abstract: *This paper presents the calibration and performance characterization of a high-pressure jet supply system developed for experimental investigations of powered wind tunnel models. The system supplies high-pressure air through a custom flow-through internal strain-gage balance to interchangeable sonic and supersonic nozzles mounted on the wind tunnel model. Tests conducted under no-main-flow conditions evaluated the transient response of the system, quantified pressure losses along the internal flow path, determined actual jet characteristics from direct thrust measurements, and assessed nozzle operating regimes. The obtained results provide essential baseline data on the internal flow behavior and jet performance. These data will support reliable interpretation and analysis of phenomena during subsequent wind tunnel tests with powered models.*

Keywords: *powered wind tunnel model; jet thrust; flow-through balance; pressure losses; reaction control system.*

1. INTRODUCTION

Powered wind tunnel testing plays a critical role in the development of aerospace vehicles, particularly for configurations relying on reaction control systems (RCS), or other propulsion-based control mechanisms. These tests enable the simulation of jet interactions with external flow, providing essential data on aerodynamic interference, thrust vectoring effectiveness, and overall vehicle stability and control under representative flight conditions [1]. Accurate replication of jet exhaust or control thrusters is challenging due to the need for precise matching of jet pressure ratios, mass flow rates, and plume characteristics while integrating high-pressure supply systems within constrained model geometries without compromising force and moment measurements [2,3].

Traditional approaches to jet simulation in wind tunnels often employ cold or heated gas routed through the model support system [2]. Previous studies have highlighted the importance of detailed calibration of jet supply systems to quantify pressure losses, transient response, and actual delivered jet performance. For instance, investigations into RCS jet interactions for planetary entry vehicles, such as the Mars Science Laboratory, underscored the need for high-fidelity simulation to reduce uncertainties in control authority and validate computational predictions [4]. Flow-through balances are utilized to accommodate the high-pressure air supply while simultaneously measuring the resulting aerodynamic loads and jet thrust [5]. Recent advancements in flow-through balance designs have enabled more accurate isolation of jet thrust from external aerodynamic forces in powered wind tunnel testing [6].

At the VTI, ongoing research into side jet interactions on slender missile configurations has necessitated the development of a dedicated high-pressure jet supply system. This system integrates a custom flow-through internal strain-gauge balance capable of delivering high-pressure air to interchangeable sonic and supersonic nozzles mounted on the wind tunnel model [7]. The present paper focuses on the calibration and performance of this high-pressure jet supply system. Key objectives include evaluating the transient response, quantifying pressure losses along the internal flow path, and determining actual jet characteristics via direct thrust measurements. These baseline data are vital for reliable interpretation of powered wind tunnel test results.

Corresponding author: B. Ilić;
E-mail: biljana.ilic@icloud.com

DOI: 10.5937/OTEH26005I

2. EXPERIMENTAL SETUP

The details of the test facility, test model, high-pressure jet supply system and the associated measurement techniques are given in the following subsections.

2.1. Test Facility

The test facility is the VTI Belgrade T-38 wind tunnel [8]. The T-38 is a large-scale blowdown wind tunnel designed to fulfill testing requirements across a Mach number range of 0.2 to 4.0. A Reynolds number of up to 100×10^6 per meter is achieved via a controllable stagnation pressure range of 1.2 bar to 15 bar [9–11]. The 1.5 m × 1.5 m test section features a 2-DOF model support system, which permits model movement within ±20º in pitch [12] and ±720 º in roll [13].

The flow is established by discharging compressed air from 2600 m^3 storage tanks, pressurized up to 20 bar, into the atmosphere, yielding a maximum run duration of 60 s. A solid-wall test section is used for subsonic and supersonic testing, where the Mach number is set by a second throat and a flexible nozzle [14], respectively. For transonic testing, a variable-porosity test section [15] with an ejector-assisted blow-off system for active Mach number control is inserted into the wind tunnel circuit.

2.2. Test Model

The generic missile model of VTI [16] is modified to accommodate a high-pressure supply and measurement system for powered wind tunnel testing. It consists of the ogive nose cone, a cylindrical fuselage, and four wrap-around fins. The model has a nominal body diameter of D = 64 mm and a slenderness ratio of L/D = 21.6. The cross-sectional view of the model mounted on the model support sting is shown in Figure 1.

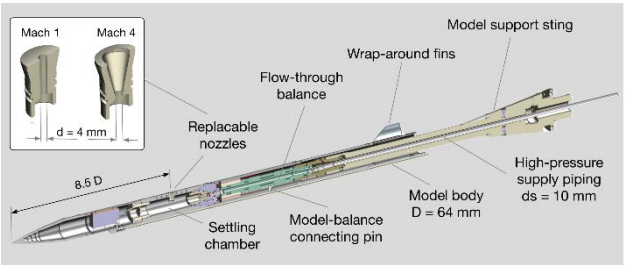


Figure 1 Powered wind tunnel model

The forward part of the model houses the settling chamber which is equipped with a nozzle. Its exit is positioned 8.5D downstream of the tip of the model nose. The nozzle body is threaded into the holder so that it can be easily replaced. Two different nozzles were designed and produced, both having a throat diameter of 4 mm, designed for Mach 1 and Mach 4 exit speeds.

A flow-through balance is integrated into the support sting, with the model mounted onto the balance via a connecting pin. This configuration prevents physical contact between the model and the support sting. Consequently, all mechanical loads acting on the model – including external aerodynamic forces and internal jet propulsion forces – are transmitted exclusively to the balance.

2.3. High-Pressure Supply System

Compressed air for powered model testing is prepared in an adjacent facility near the VTI T-38 wind tunnel. The plant utilizes two Bauer compressor units operating independently or in parallel at a maximum operating pressure of 270 bar. Initial moisture separation occurs within the compressors, followed by final drying via two aluminosilicate desiccant dryers. The conditioned air is stored at a maximum pressure of 200 bar in 14 reservoirs, providing a total volume of 9.8 m^3 (0.7 m^3 each).

The air preparation plant is linked to the VTI T-38 wind tunnel hall via a dedicated pipeline, consisting of metallic tubes with an inner diameter (ID) of 63.5 mm. Supply pressure entering the pipeline is modulated up to a maximum pressure of 150 bar using control valves located on a control panel positioned adjacent to the reservoirs.

A valve panel positioned near the wind tunnel test section enables the air flow to the model. The pipeline terminal is connected to this panel instrumentation via a 32 mm thermoplastic hose with a maximum operating pressure of 310 bar. The panel houses a computer-controlled solenoid valve (550 bar, 13 mm ID) and two manual isolation valves (350 bar, 25 mm ID) arranged in series and parallel. Upstream pressure is monitored by a 160-bar manometer. Downstream, a 25.8 mm ID thermoplastic hose (280 bar rating) routes the air to the model support mechanism, using a 6 m length for subsonic/supersonic testing or a 10 m length for transonic configurations.

Air is routed through the model support strut via a thermoplastic hose (16.3 mm ID, 140 bar rating), which connects to the upstream hose through a quick-disconnect threaded coupling (300 bar rating) for rapid assembly. The upper end of this hose exits the strut and terminates at a flexible rubber pneumatic hose (8 mm ID, 300 bar). The hose spans the junction between the fixed and moving parts of the model support. Its forward end connects to a pneumatic tube (10 mm ID, 200 bar rating) routed through an opening in the conical section of the support sting, establishing the compressed air flow path to the model.

Compressed air is delivered into the model interior via a pneumatic tube passing through the central bore of the support sting. The forward end of the tube connects to a flow-through balance. An internal axial channel (10 mm ID) along the balance body routes the airflow through a downstream tube (10 mm ID) into the settling chamber (44 mm ID, 143 mm length). The flow is then accelerated and discharged to the atmosphere through a nozzle.

2.4. Measurement Techniques and Equipment

For the jet supply system calibration, two measurement techniques were employed: jet reaction force measurement and jet supply flow measurements.

Force measurement was performed utilizing the VTI 1.5” 385 five-component flow-through internal strain-gauge balance. The normal force component (N) features a full-scale range of 2000 N with an accuracy of 0.144% of full scale; notably, only this component was relevant for the present measurement. Furthermore, calibration procedures

verified the balance accuracy under loads combined with internal airflow at a maximum pressure of 60 bar.

The jet supply flow is characterized by total pressure (p_0), static pressure (p), and total temperature (T_0). The mass flow rate is subsequently derived from these properties via standard isentropic relations.

Total and static pressures are acquired at the same axial station immediately upstream of the settling chamber using a Pitot probe and a wall pressure tap, respectively (Figure 2). These sensors are pneumatically connected to model-support-mounted miniature Entran pressure transducers, each featuring a measurement range of 70 bar and an accuracy of 0.05% of full scale.

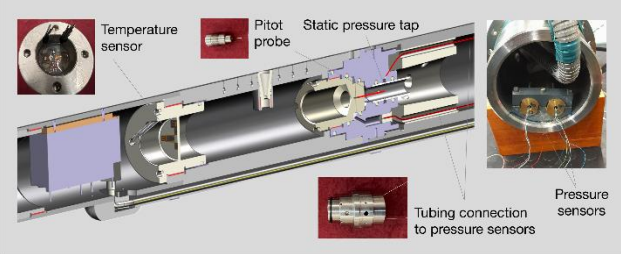


Figure 2 Jet supply flow measurements

The total temperature is measured in the settling chamber via a custom VTI half-bridge Wheatstone sensor. The circuit incorporates two active, high-pressure-rated ETG-50AE gauges (50 Ω ± 0.3%) and two precision resistors (47 Ω ± 0.1%), providing a 300 K measurement range with an accuracy of 0.2% of full scale. Dual-gauge flow exposure provides excellent common-mode rejection of strain and lead-resistance artifacts. Furthermore, the opposed-arm configuration linearizes bridge output and minimizes self-heating errors during constant-voltage operation.

2.5. Data Acquisition and Synchronization

The Pacific Instruments Series 6000 (PI6000) was utilized for high-bandwidth analog signal acquisition. All analog channels from the balance and jet supply flow sensors were conditioned and digitized by PI6000 Model 6052 input modules, each equipped with independent 16-bit A/D converters. A global sampling frequency of 400 Hz was applied across all channels. To suppress aliasing, each channel was filtered using an integrated four-pole low-pass Butterworth filter with a 30 Hz cutoff frequency.

System synchronization was managed via a PI6000 Model E6094A IRIG time-code reader, which decoded the IRIG-B signal and distributed the master sample clock, restricting intra-chassis analog skew to below 50 ns.

3. DATA PROCESSING

Evaluating the jet performance requires an accurate determination of the pneumatic state at the nozzle inlet. Compressed air routes through the internal balance into a settling chamber upstream of the nozzle. Because of frictional resistance along the internal conduits and expansion losses in the settling chamber, the pressure reaching the nozzle inlet drops substantially below the supply source pressure. To account for these losses, a mathematical methodology is developed below to calculate both the mass flow rate and the true stagnation (jet) pressure at the nozzle entry.

The mass flow rate ($\dot{m}_{in}$) delivered to the settling chamber is determined through the isentropic relations given in Eqn. (1), which utilize the jet supply flow parameters acquired just upstream of the chamber:

$$\dot{m}_{in} = \sqrt{\frac{2\kappa}{R(\kappa-1)}} A_{in} \frac{p_0}{\sqrt{T_0}} \left(\frac{p}{p_0}\right)^{\frac{1}{\kappa}} \sqrt{1-\left(\frac{p}{p_0}\right)^{\frac{\kappa-1}{\kappa}}} \quad (1)$$

where A_{in} is the inlet pipe flow area, κ is the specific heat ratio for air, and R is the specific gas constant for air. Recording these specific parameters allows for a complete thermodynamic characterization of the internal flow prior to its entry into the settling chamber.

Upon initiating the jet supple flow, the internal chamber dynamics undergo a transient phase. Steady-state behavior is achieved once the mass flow entering the chamber balances the mass flow discharging through the nozzle throat ($\dot{m}_{jet}$). Assuming choked conditions at the nozzle, this discharge mass flow becomes a function exclusively of the throat area (A_{th}) and the inlet properties (p_{jet}, T_0), as formulated in Eqn. (2):

$$\dot{m}_{jet} = \sqrt{\frac{\kappa}{R}} \left(\frac{2}{\kappa+1}\right)^{\frac{\kappa+1}{2(\kappa-1)}} A_{th} \frac{p_{jet}}{\sqrt{T_0}} \quad (2)$$

Under steady-state conditions, the settling chamber pressure (p_{sc}) represents an ideal jet pressure, derived by equating the mass flow rates from Eqns. (1) and (2). The actual stagnation pressure at the nozzle inlet (p_{jet}) is subsequently related to this ideal value by subtracting the internal pressure losses (Δp_{sc}), as expressed in Eqn. (3):

$$p_{jet} = p_{sc} - \Delta p_{sc} \quad (3)$$

Although the ideal jet pressure (p_{sc}) serves as a theoretical baseline, the true stagnation pressure (p_{jet}) at the nozzle inlet must incorporate irreversible losses within the settling chamber. To achieve an accurate determination of p_{jet}, the analytical model is coupled with empirical data by correlating the measured jet reaction force (F_{jet}) with the thrust equation, Eqn. (4):

$$F_{jet} = \dot{m}_{jet} v_e + (p_e - p_{inf}) A_e \quad (4)$$

Within this framework, p_{jet} serves as the independent variable required to close the system of equations. Given that the nozzle operates in a choked state, its exit Mach number (M_e) is first computed numerically via the isentropic area-Mach relation, Eqn. (5):

$$\frac{A_e}{A_{th}} = \left(\frac{\kappa+1}{2}\right)^{-\frac{\kappa+1}{2(\kappa-1)}} \cdot \frac{\left(1+\frac{\kappa-1}{2}M_e^2\right)^{\frac{\kappa+1}{2(\kappa-1)}}}{M_e} \quad (5)$$

The nozzle exit temperature (T_e) is then calculated using the resolved M_e and the measured settling chamber total temperature (T_0) via the isentropic relation, Eqn. (6):

$$T_e = T_0 \left(1 + \frac{\kappa-1}{2} M_e^2\right)^{-1} \quad (6)$$

The exit static temperature (T_e) is subsequently utilized to determine the flow velocity at the nozzle exit (v_e) via the following relation, Eqn. (7):

$$v_e = M_e\sqrt{\kappa R T_e} \tag{7}$$

By substituting these thermodynamic dependencies and the mass flow rate relation from Eqn. (2) into the thrust equation, Eqn. (4), p_{jet} is solved numerically to match the experimentally measured reaction force (F_{jet}). This approach ensures that all internal chamber losses are implicitly captured within the resolved p_{jet} value.

The nozzle exit static pressure (p_e) is calculated assuming an isentropic expansion from the jet pressure (p_{jet}) to the exit Mach number (M_e), Eqn. (8):

$$p_e = p_{jet}\left(1 + \frac{\kappa-1}{2}M_e^2\right)^{-\frac{\kappa}{\kappa-1}} \tag{8}$$

For calibration tests conducted without wind tunnel flow, the ambient pressure term (p_{inf}) in Eqn. (4) is taken as the local atmospheric pressure.

4. RESULTS

To isolate the characteristics of the jet supply circuit from external aerodynamic influences, calibration tests were conducted with the model mounted in the VTI T-38 test section under no-wind-tunnel-flow conditions (Figure 3).



Figure 3 Powered model mounted in the VTI T-38 wind tunnel

This approach ensures that the recorded pressure and temperature fluctuations are solely a function of the internal flow physics and valve actuation. Consequently, this methodology serves to calibrate the jet supply system, enabling a comprehensive evaluation of both its transient and steady-state performance characteristics.

4.1. Transient Performance

The previously established analytical framework assumes a steady-state equilibrium between the supply circuit and the nozzle exit. However, in practical wind tunnel testing, the time required to attain this equilibrium represents a critical operational constraint. This section evaluates the temporal behavior of the jet supply system, focusing specifically on the pneumatic latency and the filling dynamics of the settling chamber.

The test sequence was executed across nine discrete pressure steps, increasing the supply pressure (p_s) from 20 bar to 60 bar in 5 bar increments. For each step, data acquisition was triggered simultaneously with the opening of the computer-controlled solenoid valve. The measured quantities were continuously recorded for a 10-second duration, ensuring a sufficient window to capture the entire transition from the initial rest state to a stabilized steady-state plateau. All data channels were acquired at a sampling frequency of 400 Hz. This entire testing sequence was first performed for the Mach 1 nozzle configuration and subsequently repeated for the Mach 4 nozzle.

Figure 4 illustrates the transient mass flow rate ($\dot{m}_{in}$) response for the Mach 1 nozzle configuration across the evaluated range of supply pressures (p_s). To suppress experimental noise while preserving the transient peak characteristics, the raw time-series data were conditioned using a second-order Savitzky-Golay filter with a 50-point moving window (corresponding to 0.125 s).

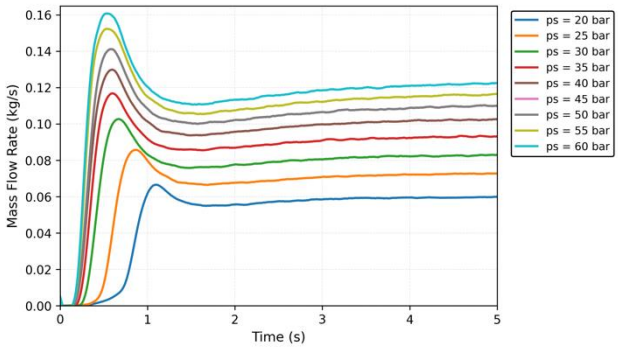


Figure 4 Transient response of the jet supply circuit

Comparative testing revealed no significant discrepancy in transient response between the Mach 1 and Mach 4 nozzle configurations. This indicates that pneumatic latency and filling dynamics are dominated by the upstream supply circuit and chamber volume rather than nozzle geometry.

The time-dependent mass flow rate ($\dot{m}_{in}$) exhibits several distinct operational phases. Following the valve trigger, a distinct dead time occurs before initial flow detection. This latency is inversely proportional to the supply pressure – decreasing from 0.5 s at 20 bar to 0.2 s at 60 bar – and is attributed to the pressure wave propagation time through the internal piping. Post-latency, the flow exhibits a steep gradient ($d\dot{m}_{in}/dt$) leading to a significant transient overshoot. At 60 bar, the mass flow peaks at approximately 0.16 kg/s, which is nearly 33% higher than its eventual steady-state value.

This overshoot stems directly from the volumetric filling of the settling chamber. Initially, the maximum pressure differential between the supply line and the empty chamber drives a high inflow, while the nozzle exit flow is restricted by the low chamber pressure. As the chamber fills, the rising internal pressure (p_{sc}) simultaneously reduces the inflow rate and increases the nozzle discharge rate. Equilibrium is established roughly 4.0 s after the initial rise, when the filling and exhaust mass flows balance.

Consequently, this dynamics dictate the wind tunnel testing protocol. To ensure true steady-state conditions, a minimum dwell time of 4.0 s is required post-activation before recording valid aerodynamic data. This delay ensures the pneumatic system has fully transitioned into the steady-state regime assumed by the analytical model.

4.2. Steady-State Performance

This section characterizes the steady-state pneumatic efficiency of the jet supply circuit. By coupling the analytical framework from Section 3 with empirical force and pressure data, internal losses between the upstream supply lines and the settling chamber are quantified for both the Mach 1 and Mach 4 nozzle configurations.

The tests were conducted across nine discrete supply pressure steps (p_s= 20 bar to 60 bar in 5 bar increments). Steady-state data acquisition simultaneously captured the total duct pressure (p_0), static duct pressure (p), total temperature (T_0), and jet reaction force (F_{jet}). To exclude the transient filling dynamics, data logging was initiated only after a 4-seconds post-activation dwell time. For each pressure step, parameters were sampled at 400 Hz for 10 s. This approach yielded a statistically robust dataset that minimized high-frequency pneumatic noise and ensured a precise determination of the mean properties.

Prior to testing, system integrity was verified via a pressure-decay leak check. The isolated circuit was pressurized to 60 bar and monitored for 10 minutes using the internal transducers (p_0, p); no detectable pressure drop occurred. This verified zero mass leakage into the model interior, preserving force measurement accuracy.

The Mach 1 and Mach 4 nozzle comparative performance at tested supply pressures are summarized in Figure 5. The total pressure drop across the system (Δp_{tot}) is decomposed into two primary components: losses within the piping upstream of the model (Δp_{up}) and losses generated inside the settling chamber itself (Δp_{sc}). The latter is resolved by comparing the ideal jet pressure (Δp_{sc}) with the actual jet stagnation pressure (Δp_{jet}) according to Eqn. (3) of the analytical model.

Although the upstream piping constitutes the largest portion of the total pressure drop, the settling chamber contribution remains significant. Specifically, for the Mach 1 nozzle, the settling chamber's share of total losses increases from 21.0% at p_s= 20 bar to 31.7% at p_s= 60 bar. This trend indicates that internal chamber inefficiencies driven by intensified turbulence and irreversible expansion become increasingly dominant at higher mass flow rates.

The jet stagnation pressure p_{jet} as a function of supply pressure p_s for both nozzle configurations is presented in Figure 6, together with the ideal settling chamber pressure p_{sc} calculated from mass-flow continuity. At the lowest supply pressure (p_s = 20 bar), both nozzles deliver nearly identical jet stagnation pressures ($p_{jet} \approx$ 14.8 bar). As supply pressure increases, however, a clear divergence emerges. The Mach 4 nozzle consistently achieves higher values of p_{jet} than the Mach 1 nozzle, with the difference becoming progressively larger above 40 bar. At p_s = 60 bar, the Mach 4 nozzle reaches $p_{jet} \approx$ 44.7 bar compared to 42.6 bar for the Mach 1 nozzle.

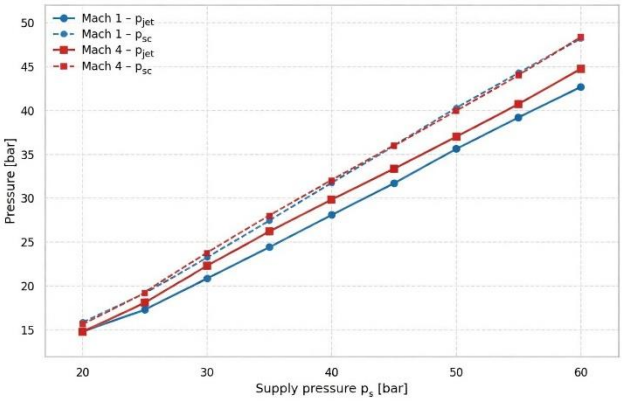


Figure 6 Comparative pressure recovery analysis

This performance advantage is directly attributable to differences in internal flow behavior within the settling chamber. As shown in Figure 5, the absolute internal pressure losses ($\Delta p_{up} + \Delta p_{sc}$) are lower for the Mach 4 nozzle at higher supply pressures, despite nearly identical upstream losses in both configurations. The contribution of settling chamber losses (orange segments) is visibly smaller for the Mach 4 geometry across the entire range, and the gap widens with increasing mass flow rate. Consequently, the deviation between the measured jet stagnation pressure p_{jet} and the ideal settling chamber pressure p_{sc} remains smaller for the supersonic nozzle, indicating reduced irreversible losses associated with flow expansion and turbulence inside the chamber. In addition, this deviation demonstrates that internal flow losses are successfully captured by the force-based method.

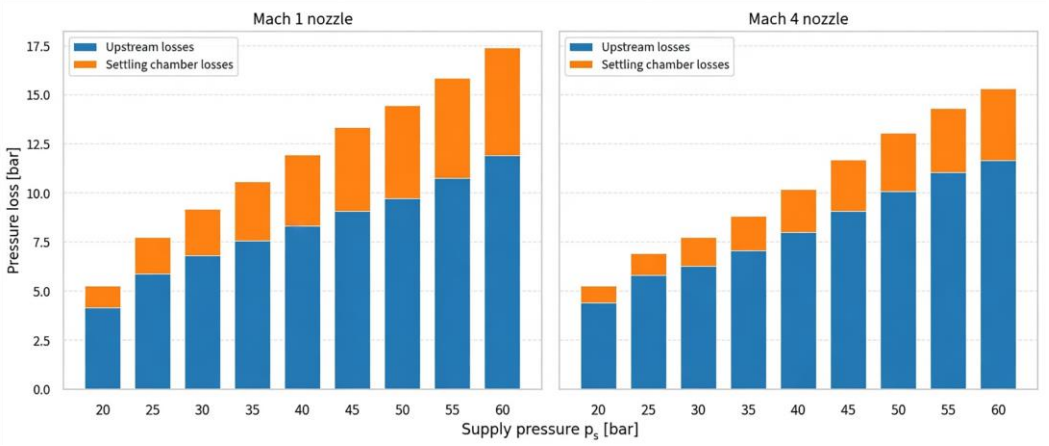


Figure 5 Pressure loss contribution analysis

Figure 7 presents the directly measured jet reaction force F_{jet} as a function of the jet stagnation pressure p_{jet} determined from the thrust equation for both nozzle configurations under atmospheric (no-wind-tunnel-flow) conditions. A clear linear relationship is observed for both the Mach 1 and Mach 4 nozzles, consistent with the theoretical thrust equation for choked nozzles. The Mach 4 nozzle exhibits a steeper slope, producing higher reaction force at the same jet stagnation pressure due to its higher exhaust velocity resulting from supersonic expansion in the divergent section. The data points remain well within the uncertainty bands across the entire tested range. The two curves intersect at low jet stagnation pressures; below this intersection the Mach 1 nozzle yields slightly higher force, while above approximately 20 bar the trend reverses and the Mach 4 nozzle maintains progressively higher reaction force with increasing p_{jet}.

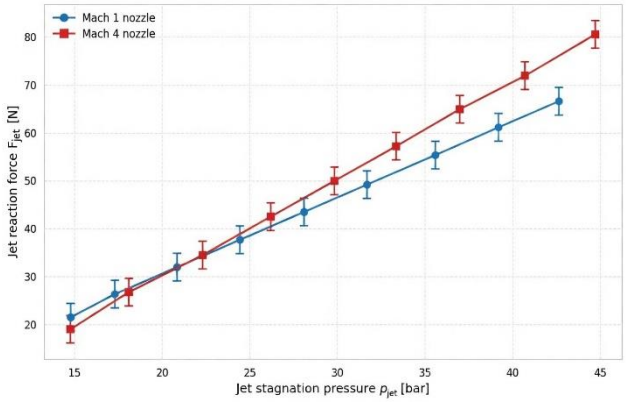


Figure 7 Jet reaction force under atmosphere conditions

In the wind tunnel, the nozzle exhausts into a local test section static pressure that can differ significantly from the atmospheric pressure present during the static calibration. Consequently, the jet thrust (F_{jet}) obtained here must be adjusted analytically using the classical thrust equation. In the pressure thrust component $(p_e - p_{inf})A_e$, the atmospheric reference pressure is replaced with the actual local test section pressure, allowing the true jet thrust force to be isolated in the subsequent wind tunnel tests.

5. CONCLUSIONS

The high-pressure jet supply system was calibrated under no-main-flow conditions using direct jet reaction force measurements. A dwell time of 4 s was required to reach steady-state conditions in the internal settling chamber. Upstream piping losses represented the dominant contribution to the total internal pressure drop for both nozzle configurations. Settling chamber losses were lower for the Mach 4 nozzle and increased with supply pressure for both nozzles. The Mach 4 nozzle delivered higher jet stagnation pressure and jet reaction force than the Mach 1 nozzle at supply pressures above 25 bar. A linear relationship between jet reaction force and jet pressure was obtained for both nozzles, consistent with the theoretical thrust equation. The force-based method enabled determination of actual jet stagnation pressure, providing validated baseline data for powered wind tunnel testing.

Acknowledgements

This work was supported by the Ministry of Science, Technological Development and Innovation, Republic of Serbia (Contract No 451-03-34/2026-03/200325).

REFERENCES

[1] A.A. Dyakonov, M. Schoenenberger, W.I. Scallion, J.W. Van Norman, L.A. Novak, C.Y. Tang, Aerodynamic Interference Due to MSL Reaction Control System, in: 41st AIAA Thermophysics Conference, San Antonio, 2009.

[2] B. Stahl, H. Emunds, A. Gülhan, Experimental investigation of hot and cold side jet interaction with a supersonic cross-flow, Aerosp. Sci. Technol. 13 (2009) 488–496.

[3] A. Kovar, E. Schülein, Effect of Side Jets in a Supersonic Flow Measured and Calculated on a Flat Plate and a Generic Missile Configuration, Innovative Missile Systems Paper 37 (2006) 1–16.

[4] C.T. Johansen, L. Novak, B.F. Bathel, S.W. Ashcraft, P.M. Danehy, Mars Science Laboratory Reaction Control System Jet Computations with Visualization and Velocimetry, J. Spacecr. Rockets 50 (2013) 1183–1195.

[5] J. Melton, K. James, J.D. Flamm, K. Long, Estimating Flow-Through Balance Momentum Tares with CFD (Invited), in: 54th AIAA Aerospace Sciences Meeting, American Institute of Aeronautics and Astronautics, 2016.

[6] D.E. Burns, P.A. Parker, C.M. Cagle, K.G. Toro, B. Kleb, V.M. Hawke, New Flow-Through Wind-Tunnel Balance for Retropropulsion Testing, J. Spacecr. Rockets 59 (2022) 1926–1933.

[7] B. Ilić, M. Samardžić, G. Ocokoljić, Integrated multi-technique experimental setup for wind tunnel investigation of side jet interaction with crossflow, Aerosp. Sci. Technol. 177 (2026) 112705.

[8] B. Ilić, G. Ocokoljić, M. Samardžić, J. Isaković, Upgrade of the VTI T-38 Blowdown Trisonic Test Facility: Wind Tunnel Control System, in: ICAS Proceedings - 34th Congress of the International Council of the Aeronautical Sciences, Florence, 2024, ICAS2024_0456.

[9] B. Ilić, M. Miloš, J. Isakovic, Cascade nonlinear feedforward-feedback control of stagnation pressure in a supersonic blowdown wind tunnel, Measurement 95 (2017) 424–438.

[10] B. Ilić, M. Milosavljević, J. Isaković, M. Miloš, Stagnation Pressure Transient Control in a High-Pressure Supersonic Blowdown Wind Tunnel Test Facility, 32nd DAS, Stary Smokovec, 2015: pp. 82–83.

[11] B. Ilić, M. Miloš, M. Milosavljević, J. Isaković, Model-Based Stagnation Pressure Control in a Supersonic Wind Tunnel, FME Transactions 44 (2016) 1–9.

[12] B. Ilić, M. Milosavljević, S. Krstić, G. Ocokoljić, D. Damljanović, Control System Design and Integration of a Blowdown Wind Tunnel Model Support Pitch Mechanism, OTEH 2022 - Proceedings, Belgrade, 2022: pp. 210–216.

[13] D. Vuković, B. Ilić, M. Milosavljević, Upgrade of the Roll-Angle-Setting Mechanism on the Model Support System in the T-38 Wind Tunnel in VTI, OTEH 2011 - Proceedings, 2011: pp. 23–28.

[14] B. Ilić, M. Milosavljević, FPGA-based Embedded System for Wind Tunnel Variable-Geometry Nozzle Positioning, Scientific Technical Review 69 (2019) 3–9.

[15] G.M. Elfstrom, B. Medved, W.J. Rainbird, Wave cancellation properties of a splitter-plate porous wall configuration, J. Aircr. 26 (1989) 920–924.

[16] M. Samardžić, N. Vujić, B. Ilić, G. Ocokoljić, Experimental Results from the Missile Model Test Campaign in the VTI T-38 Wind Tunnel, OTEH 2024 - Proceedings, pp. 43–49.